Order online now!

www.rockland.com
tech@rockland.com
+1 484.791.3823

Datasheet for 611-145-002

Rabbit IgG (H&L) Antibody DyLight™ 800 Conjugated

Overview

Description:	Goat Anti-Rabbit IgG (H&L) Antibody DyLight™ 800 Conjugated - 611-145-002
Item No.:	611-145-002
Size:	100 µg
Applications:	Dot Blot, ELISA, WB, EMSA, IHC, IP
Reactivity:	Rabbit
Host Species:	Goat

Product Details

Background:	Anti-Rabbit IgG Antibody DyLight™800 generated in goat detects rabbit IgG. Secreted as part of the adaptive immune response by plasma B cells, immunoglobulin G constitutes 75% of serum immunoglobulins. Immunoglobulin G binds to viruses, bacteria, as well as fungi and facilitates their destruction or neutralization via agglutination (and thereby immobilizing them), activation of the compliment cascade, and opsonization for phagocytosis. The whole IgG molecule possesses both the F(c) region, recognized by high-affinity Fc receptor proteins, as well as the F (ab) region possessing the epitope-recognition site. Both heavy and light chains of the antibody molecule are present. Secondary Antibodies are available in a variety of formats and conjugate types. When choosing a secondary antibody product, consideration must be given to species and immunoglobulin specificity, conjugate type, fragment and chain specificity, level of cross-reactivity, and host-species source and fragment composition. This Anti-Rabbit IgG (H&L) is conjugated to DyLight™800.
Synonyms:	Goat anti-Rabbit IgG Antibody DyLight™800 Conjugation, Goat anti-Rabbit IgG DyLight™ 800 Conjugated Antibody
Host Species:	Goat
Specificity:	IgG (H&L)
Conjugate:	DyLight™ 800
Clonality:	Polyclonal
Format:	IgG
F/P Ratio:	1.7

Target Details

Reactivity:	Rabbit
Immunogen:	Rabbit IgG whole molecule
Purity/Specificity:	This product was prepared from monospecific antiserum by immunoaffinity chromatography using Rabbit IgG coupled to agarose beads followed by conjugation to fluorochrome and extensive dialysis against the buffer stated above. Assay by immunoelectrophoresis resulted in a single precipitin arc against anti-Goat Serum, Rabbit IgG and Rabbit Serum. This antibody will react with heavy chains of Rabbit IgG and with light chains of most Rabbit immunoglobulins.
Relevant Links:	• 611-145-022 SDS

Application Details

Tested Applications:	Dot Blot, ELISA, WB
Suggested Applications:	EMSA, IHC, IP (Based on references)
Application Note:	Anti-Rabbit IgG Antibody DyLight™800 has been tested by ELISA, dot blot, and western blot and is designed for immunofluorescence microscopy, fluorescence based plate assays (FLISA) and fluorescent western blotting. This product is also suitable for multiplex analysis, including multicolor imaging, utilizing various commercial platforms. The emission spectra for this DyLight™ conjugate match the principle output wavelengths of most common fluorescence instrumentation.
Assay Dilutions:	All assays should be optimized by the user. Recommended dilutions (if any) may be listed below.
FLISA:	>1:20,000
IF:	>1:5,000
WB:	>1:10,000

Formulation

Physical State:	Lyophilized
Concentration:	1.0 mg/mL by UV absorbance at 280 nm
Buffer:	0.02 M Potassium Phosphate, 0.15 M Sodium Chloride, pH 7.2
Preservative:	0.01% (w/v) Sodium Azide
Stabilizer:	10 mg/mL Bovine Serum Albumin (BSA) - Immunoglobulin and Protease free

Reconstitution Volume:	100 µL
Reconstitution Buffer:	Restore with deionized water (or equivalent)

Shipping & Handling

Shipping Condition:	Ambient
Storage Condition:	Store vial at 4° C prior to restoration. For extended storage aliquot contents and freeze at -20° C or below. Avoid cycles of freezing and thawing. Centrifuge product if not completely clear after standing at room temperature. This product is stable for several weeks at 4° C as an undiluted liquid. Dilute only prior to immediate use.
Expiration:	Expiration date is one (1) year from date of receipt.

Images

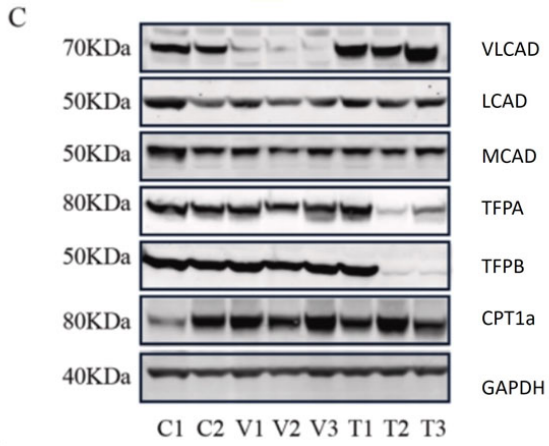

Western Blot

C. Representative western blots, original blots are shown in (supplementary Fig S8-9). And densitometric quantification of relative protein levels from western blots. Data are depicted as mean ± SD, n = 3, **P < 0.01, ***P < 0.001 and ****P < 0.0001 by one-way ANOVA. Intracellular transport, activation, mitochondrial transport, β-oxidation, carnitine shuttle, and auxiliary proteins. The primary antibodies used as follows: VLCAD 1:1000, MCAD 1:1000, LCAD 1:1000, TFPa 1:500, TFPb 1:3000, CPT1α 1:1000, and GAPDH 1:30,000 dilutions overnight at 4 °C. The membranes were then incubated with fluorescent conjugated secondary antibodies for 1 h; DyLight 800 conjugated goat Anti-Rabbit IgG (611-145-002), DyLight 680 conjugated goat Anti-Rabbit IgG (611-144-003), DyLight 800 conjugated goat Anti-Mouse IgG (610-145-002), and DyLight 680 conjugated donkey Anti-Mouse IgG (610-744-124). Fig 1. PMID: 33725513.

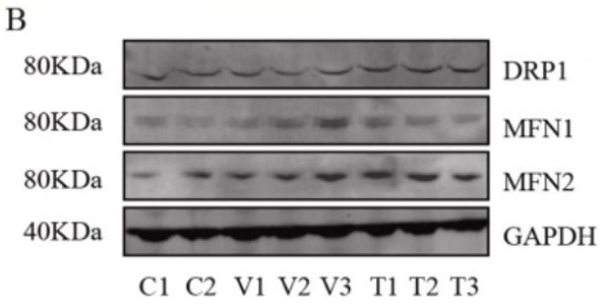

Western Blot
Assessment of mitochondrial fusion and fission. B. Representative western blots (original blots are shown in supplementary Fig. S10) and quantification of MFN1/2 and DRP1. No significant changes in the relative levels of proteins that facilitate mitochondrial fusion (MFN1/2) and fission (DRP1) between non-disease (control) and mutant primary fibroblasts. Data are depicted as mean ± SD, n = 3. The primary antibodies used as follows: MFN1 1:400, MFN2 (1:400, DRP1 1:100 and GAPDH 1:30,000 dilutions overnight at 4 °C. The membranes were then incubated with fluorescent conjugated secondary antibodies for 1 h; DyLight 800 conjugated goat Anti-Rabbit IgG (611-145-002), Antibody DyLight 680 conjugated Anti-Rabbit IgG made in goat (611-144-003), DyLight 800 conjugated goat Anti-Mouse IgG (610-145-002), and DyLight 680 conjugated donkey Anti-Mouse IgG (610-744-124). Fig 3. PMID: 33725513.

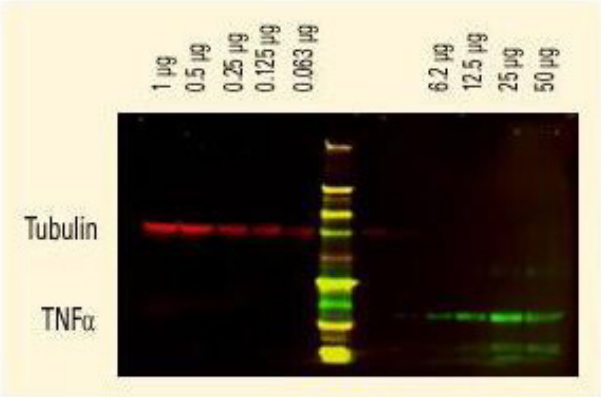

Western Blot
DyLight™ dyes can be used for two-color western blot detection with low background and high signal. Anti-tubulin was detected using a DyLight™ 680 conjugate. Anti-TNFa was detected using a DyLight™ 800 conjugate. The image was captured using the Odyssey® Infrared Imaging System developed by LI-COR.

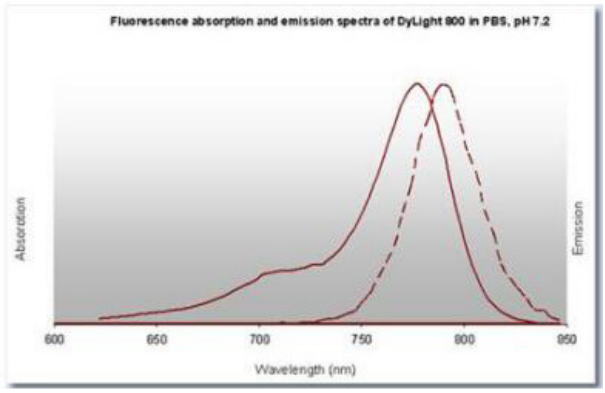

Diagram
DyLight™ 800 Fluorescence Spectra.

Diagram
Properties of DyLight™ Fluorescent Dyes.

Emission	Color	DyLight™ Dye	Ex/Em (nm)	ε (M^{-1} cm^{-1})	Similar Dyes
Blue		**405**	**400/420**	**30,000**	**Alexa™ 405, Cascade Blue**
Green		488	493/518	70,000	Alexa™ 488, Cy2®, FITC
Yellow		549	550/568	150,000	Alexa™ 546, Alexa 555, Cy3®,TRITC
Red		649	646/674	250,000	Alexa™ 647, Cy5®
Near Infrared		680	682/715	140,000	Alexa™ 680, Cy5.5®, IRDye™ 700
Infrared		800	770/794	270,000	IRDye™ 800

References

- Velde HM et al. Exome variant prioritization in a large cohort of hearing-impaired individuals indicates IKZF2 to be associated with non-syndromic hearing loss and guides future research of unsolved cases. *Hum Genet.* (2024)
- Smolak P et al. Target Cell Activation of a Structurally Novel NOD-Like Receptor Pyrin Domain-Containing Protein 3 Inhibitor NT-0796 Enhances Potency. *J Pharmacol Exp Ther.* (2024)
- Zhao S et al. Atrial proteomic profiling reveals a switch towards profibrotic gene expression program in CREM-IbΔC-X mice with persistent atrial fibrillation. *J Mol Cell Cardiol.* (2024)
- Chen L et al. The impact of Nrf2 knockout on the neuroprotective effects of dexmedetomidine in a mice model of cognitive impairment. *Behav Brain Res.* (2024)
- Späte E et al. Downregulated expression of lactate dehydrogenase in adult oligodendrocytes and its implication for the transfer of glycolysis products to axons. *Glia.* (2024)
- Chen R et al. Destabilization of fear memory by Rac1-driven engram-microglia communication in hippocampus. *Brain Behav Immun.* (2024)
- Meng P et al. A whole transcriptome profiling analysis for antidepressant mechanism of Xiaoyaosan mediated synapse loss via BDNF/trkB/PI3K signal axis in CUMS rats. *BMC Complement Med Ther.* (2023)
- Zhou Y et al. Targeting of HBP1/TIMP3 axis as a novel strategy against breast cancer. *Pharmacol Res.* (2023)
- Yang R et al. The transcription factor HBP1 promotes ferroptosis in tumor cells by regulating the UHRF1-CDO1 axis. *PLoS Biol.* (2023)
- Zhang Y et al. Testosterone reduces hippocampal synaptic damage in an androgen receptor-independent manner. *J Endocrinol.* (2023)
- Wu W et al. SARS-CoV-2 N protein induced acute kidney injury in diabetic db/db mice is associated with a Mincle-dependent M1 macrophage activation. *Front Immunol.* (2023)
- Fornes O et al. A multimorphic mutation in IRF4 causes human autosomal dominant combined immunodeficiency. *Sci Immunol.* (2023)

- Huang M et al. Bioinformatics and network pharmacology identify promotional effects and potential mechanisms of ethanol on esophageal squamous cell carcinoma and experimental validation. *Toxicol Appl Pharmacol.* (2023)
- Cheng y et al. HBP1 inhibits the development of type 2 diabetes mellitus through transcriptional activation of the IGFBP1 gene. *Aging (Albany NY).* (2022)
- Zhang R et al. Nrf2 improves hippocampal synaptic plasticity, learning and memory through the circ-Vps41/miR-26a-5p/CaMKIV regulatory network. *Exp Neurol.* (2022)
- Tang, M et al. Paclitaxel induces cognitive impairment via necroptosis, decreased synaptic plasticity and M1 polarisation of microglia. *Pharmaceutical Biology* (2022)
- Sun, Z et al. Casein kinase 2 attenuates brain injury induced by intracerebral hemorrhage via regulation of NR2B phosphorylation. *Frontiers in Cellular Neuroscience* (2022)
- Wang, X et al. RNA-based therapies in animal models of Leber congenital amaurosis causing blindness. *Precision Clinical Medicine* (2022)
- Chen H et al. Fragile X Mental Retardation Protein Mediates the Effects of Androgen on Hippocampal PSD95 Expression and Dendritic Spines Density/Morphology and Autism-Like Behaviors Through miR-125a. *Frontiers in Cellular Neuroscience* (2022)
- Joshi, H et al. L-plastin enhances NLRP3 inflammasome assembly and bleomycin-induced lung fibrosis. *Cell Reports* (2022)
- Winter JM et al. Collateral deletion of the mitochondrial AAA+ ATPase ATAD1 sensitizes cancer cells to proteasome dysfunction. *Elife.* (2022)
- Zhang H et al. Pharmacological suppression of Nedd4-2 rescues the reduction of Kv11.1 channels in pathological cardiac hypertrophy. *Front Pharmacol.* (2022)
- Mi S et al. CaMKII is a modulator in neurodegenerative diseases and mediates the effect of androgen on synaptic protein PSD95. *Front Genet.* (2022)
- Zhang R et al. Knockdown of METTL16 disrupts learning and memory by reducing the stability of MAT2A mRNA. *Cell Death Disc.* (2022)
- Kitaoka M et al. Molecular conflicts disrupting centromere maintenance contribute to Xenopus hybrid inviability. *Curr Biol.* (2022)
- Cao Z et al. HBP1-mediated transcriptional repression of AFP inhibits hepatoma progression. *J Exp Clin Cancer Res.* (2021)
- Liu Y et al. GP73-mediated secretion of AFP and GP73 promotes proliferation and metastasis of hepatocellular carcinoma cells. *Oncogenesis.* (2021)
- Li H et al. Icaritin promotes apoptosis and inhibits proliferation by down-regulating AFP gene expression in hepatocellular carcinoma. *BMC Cancer.* (2021)
- Agulto RL et al. Autoregulatory control of microtubule binding in doublecortin-like kinase 1. *Elife.* (2021)
- Klemm LC et al. Centriole and Golgi microtubule nucleation are dispensable for the migration of human neutrophil-like cells. *Mol Biol Cell.* (2021)

- Lu HY et al. Mechanistic understanding of the combined immunodeficiency in complete human CARD11 deficiency. *J Allergy Clin Immunol.* (2021)
- Strait AA et al. Distinct immune microenvironment profiles of therapeutic responders emerge in combined TGFβ/PD-L1 blockade-treated squamous cell carcinoma. *Commun Biol.* (2021)
- Fung SY et al. MALT1-Dependent Cleavage of HOIL1 Modulates Canonical NF-κB Signaling and Inflammatory Responsiveness. *Front Immunol.* (2021)
- Xu S et al. IL-6 promotes nuclear translocation of HIF-1α to aggravate chemoresistance of ovarian cancer cells. *Eur J Pharmacol.* (2021)
- Raimo S et al. Mitochondrial morphology, bioenergetics and proteomic responses in fatty acid oxidation disorders. *Redox Biol.* (2021)
- Navarro R et al. TGF-β-induced IGFBP-3 is a key paracrine factor from activated pericytes that promotes colorectal cancer cell migration and invasion. *Mol Oncol.* (2020)
- Asthana V et al. Development of a Novel Class of Self-Assembling dsRNA Cancer Therapeutics: a Proof of Concept Investigation. *Mol Ther Oncolytics.* (2020)
- Mitra S, Bodor DL, David AF, et al. Genetic screening identifies a SUMO protease dynamically maintaining centromeric chromatin. *Nat Commun.* (2020)
- Takahashi H, Ranjan A, Chen S, et al. The role of Mediator and Little Elongation Complex in transcription termination. *Nat Commun.* (2020)
- Xue J et al. Acetylation of alpha-fetoprotein promotes hepatocellular carcinoma progression. *Cancer Lett.* (2020)
- Plana-Bonamaiso A et al. GCAP neuronal calcium sensor proteins mediate photoreceptor cell death in the rd3 mouse model of LCA12 congenital blindness by involving endoplasmic reticulum stress. *Cell Death Dis.* (2020)
- Nowinski SM et al. Mitochondrial fatty acid synthesis coordinates oxidative metabolism in mammalian mitochondria. *Elife* (2020)
- Li R et al. RNF115 deletion inhibits autophagosome maturation and growth of gastric cancer *Cell Death Dis.* (2020)
- Trevisiol A et al. Structural myelin defects are associated with low axonal ATP levels but rapid recovery from energy deprivation in a mouse model of spastic paraplegia. *PLoS Biol.* (2020)
- Day EK et al. ERK-dependent suicide gene therapy for selective targeting of RTK/RAS-driven cancers. *Mol Ther.* (2020)
- Cao et al. MDM2 promotes genome instability by ubiquitinating the transcription factor HBP1. *Oncogene* (2019)
- Hong D et al. Deletion of TMEM268 inhibits growth of gastric cancer cells by downregulating the ITGB4 signaling pathway. *Cell Death Differ.* (2019)
- Quancard J et al. An allosteric MALT1 inhibitor is a molecular corrector rescuing function in an immunodeficient patient. *Nat Chem Biol.* (2019)
- Li B et al. Isobavachalcone exerts anti‐proliferative and pro‐apoptotic effects on human liver cancer cells by targeting the ERKs/RSK2 signaling pathway. *Oncol Rep.* (2019)
- Yu S et al. RSRC1 suppresses gastric cancer cell proliferation and migration by regulating PTEN expression. *Mol Med Rep.* (2019)

- Goutierre M et al. KCC2 regulates neuronal excitability and hippocampal activity via interaction with Task-3 channels. *Cell Rep.* (2019)
- Sriramachanfran AM et al. Arkadia/RNF111 is a SUMO-targeted ubiquitin ligase with preference for substrates marked with SUMO1-capped SUMO2/3 chain. *Nat Commun.* (2019)
- Miller KE et al. Kif2a scales meiotic spindle size in Hymenochirus boettgeri. *Curr Biol.* (2019)
- Wang M et al. Native Polyacrylamide Gel Electrophoresis Immunoblot Analysis of Endogenous IRF5 Dimerization. *J Vis Exp.* (2019)
- Zhang D et al. High iodine effects on the proliferation, apoptosis, and migration of papillary thyroid carcinoma cells as a result of autophagy induced by BRAF kinase. *Biomed Pharmacother.* (2019)
- Myles et al. TNF overproduction impairs epithelial staphylococcal response in hyper IgE syndrome. *Journal of Clinical Investigation* (2018)
- Lin et al. Liver-specific deletion of Eva1a/Tmem166 aggravates acute liver injury by impairing autophagy. *Cell Death & Disease* (2018)
- Zhang et al. Amelioratory Effects of Testosterone Propionate on Age-related Renal Fibrosis via Suppression of TGF-β1/Smad Signaling and Activation of Nrf2-ARE Signaling. *Scientific Reports* (2018)
- Yu S et al. PPP2R2D, a regulatory subunit of protein phosphatase 2A, promotes gastric cancer growth and metastasis via mechanistic target of rapamycin activation. *Int J Oncol.* (2018)
- de Weerd NA et al. A hot spot on interferon α/β receptor subunit 1 (IFNAR1) underpins its interaction with interferon-β and dictates signaling. *J Biol Chem.* (2017)
- Wang et al. A positive feedback loop between Pim-1 kinase and HBP1 transcription factor contributes to hydrogen peroxide-induced premature senescence and apoptosis. *Journal of Biological Chemistry* (2017)
- Li et al. Deletion of Pdcd5 in mice led to the deficiency of placenta development and embryonic lethality. *Cell Death & Disease* (2017)
- Wang et al. Efficacy of Postnatal In Vivo Nonsense Suppression Therapy in a Pax6 Mouse Model of Aniridia. *Molecular Therapy - Nucleic Acids* (2017)
- Xia et al. Knockout of MARCH2 inhibits the growth of HCT116 colon cancer cells by inducing endoplasmic reticulum stress. *Cell Death & Disease* (2017)
- Heubl et al. GABAA receptor dependent synaptic inhibition rapidly tunes KCC2 activity via the Cl--sensitive WNK1 kinase. *Nature Communications* (2017)
- Shen et al. EMC6/TMEM93 suppresses glioblastoma proliferation by modulating autophagy. *Cell Death & Disease* (2016)
- Chen et al. HBP1-mediated Regulation of p21 Protein through the Mdm2/p53 and TCF4/EZH2 Pathways and Its Impact on Cell Senescence and Tumorigenesis. *Journal of Biological Chemistry* (2016)
- Xia D et al. MARCH2 regulates autophagy by promoting CFTR ubiquitination and degradation and PIK3CA-AKT-MTOR signaling. *Autophagy.* (2016)
- Wang W et al. PIASxα ligase enhances SUMO1 modification of PTEN protein as a SUMO E3 ligase. *J Biol Chem.* (2014)
- Wang Z et al. PHF23 (plant homeodomain finger protein 23) negatively regulates cell autophagy by promoting ubiquitination and degradation of E3 ligase LRSAM1. *Autophagy.* (2014)

- Li Y et al. A novel ER-localized transmembrane protein, EMC6, interacts with RAB5A and regulates cell autophagy. *Autophagy.* (2013)

Disclaimer